

Damage metrics for masonry bridges under scour scenarios

F. Scozzese^{1*}, E. Tubaldi², A. Dall'Asta¹

¹ School of Architecture and Design (SAAD), University of Camerino

Viale della Rimembranza, 63100, Ascoli Piceno (AP), Italy

e-mail: fabrizio.scozzese@unicam.it, andrea.dallasta@unicam.it

* Corresponding author

² Department of Civil and Environmental Engineering, University of Strathclyde, 75 Montrose Street, Glasgow, G1 1XQ, UK

e-mail: enrico.tubaldi@strath.ac.uk

Abstract

Scour constitutes a significant threat to bridges. When it is not directly measured, it can be very difficult to detect and may go unnoticed until it produces catastrophic effects. Thus, understanding the effects of scour on bridge structures is of paramount importance for the development of effective scour monitoring strategies and early warning scour systems. This paper investigates the impact of scour on masonry arch bridges, which are the bridge typology most vulnerable to such a hazard. It aims at identifying synthetic damage parameters that can be used for bridge vulnerability and risk assessment, as well as at providing information about the optimal sensor placement in a monitoring system. For this purpose, extensive numerical analyses are performed on a representative bridge prototype to quantify how different response parameters, including kinematic parameters and modal parameters (i.e., the natural frequencies, and qualitatively the transverse mode-shapes), evolve under scour scenarios of increasing severity. The most recurrent damage scenarios involving piers, spandrel walls and arches are analysed to quantify the scour levels activating the various failure mechanisms, which can be finely detected and assessed through the numerical simulations. The study results allow identifying the parameters that are most sensitive to scour and the relevant limit values of interest for risk analysis. They are also useful to inform the development of optimal monitoring strategies for masonry arch bridges exposed to scour.

Damage metrics for masonry bridges under scour scenarios

Keywords: masonry bridges; scour; monitoring; response parameters; damage states; failure; Abaqus FEM.

1. INTRODUCTION

Bridge scour poses a significant threat to transport infrastructure worldwide [1]-[7]. Scour consists in the excavation and removal of material from the bed of streams around bridge foundations due to the erosive action of flowing water under heavy floods. The loss of support and foundation settlements due to scour can induce significant damage to bridges. Among the many factors that affect the vulnerability of bridges to scour, the foundation depth and the bridge typology are important ones [7]-[11]. Masonry arch bridges, which have been the most used solution to cross waterways for centuries, are particularly vulnerable to this action [11]-[14], due to their high stiffness and the fact that they were built on shallow footings or on timber piles that have rotted with time. The number of existing masonry bridges still functioning worldwide (e.g., in Europe [12], UK [14], United States of America [6], etc.) is very high. Most of these bridges have important historical and cultural value, and thus preservation of their integrity is of paramount importance not only to avoid severe direct and indirect losses, but also to prevent the loss of cultural heritage intangible value.

The relevance of the problem is substantiated by the large number of scour-induced collapses registered in the last decades, exacerbated by the increase of extreme weather events due to climate change [15]. This is reflected in the rapid growth of scientific studies on the topic, with several works dedicated to the development of simplified and advanced modelling strategies for describing the collapse mechanisms of masonry arch bridges due to scour [10],[16]-[20].

Studies have been also conducted to better understand and describe the temporal evolution of the scour process, which is affected not only by the bridge geometrical properties, but also by the hydrological conditions of both the catchment area and the river (see e.g. [3],[21][22]).

Moreover, significant research efforts have been directed at the development of monitoring tools (see e.g. [23] - [28]) and/or strategies [29] for detecting scour developing underneath bridge piers.

On this regard, sensors for scour monitoring can be classified in two categories, depending on whether they can detect and measure directly scour at a particular location or they measure the effects of scour on the bridge. These latter can provide not only an indication of the occurrence and possibly the location and extent

Damage metrics for masonry bridges under scour scenarios

of scour, but also information about potential damage of the structure. The first category includes many sensors, e.g. scour probes, sonar devices, etc., whereas the second category includes structural health monitoring (SHM) sensors such as inclinometers, transducers, accelerometers, cameras (see e.g. [30]-[35]).

Studies on the direct measurement of scour are more numerous than those aimed at the indirect assessment of scour based on SHM sensors, which is a very challenging inverse problem, due to the fact that scour usually progresses latently, without apparent effects on the superstructure up to critical levels at which bridge stability might results strongly jeopardised. Some preliminary analyses carried out by Tubaldi et al. [17] and Scozzese et al. [18] on two real case studies have shown that pier rotations and deflections are not significant until the base of the foundation is undermined. Similarly, according to the investigations of Scozzese et al. [18], the changes in dynamic properties of the bridge become significant only when scour has significantly undermined the foundation of a pier. However, further investigations are needed to better understand the effects of scour on the various components and response parameters of masonry arch bridges. Such investigations can be useful not only for the definition of optimal monitoring strategies, but also for improving current bridge risk management systems [36]. In fact, many emergency management systems for bridges base their decision making (e.g. whether to close a bridge or not) on water levels rather than on the knowledge of the scour or of its structure-related effects. For example, in the UK water level markers corresponding to the expected 200 years return period flood [37] are placed in correspondence of bridges and used to decide on bridge closure under heavy floods. The decision making process could benefit from a deeper knowledge of the actual scour hazards and of the effects of scour.

More in general, understanding the response of masonry arch bridge components to floods and identifying demand parameters threshold corresponding to various damage levels is of paramount importance for the development of a performance-based flood engineering method for the evaluation of bridge risk. On this regard, while performance-based assessment methodologies for bridges under

the earthquake hazard are well established (see e.g. [38][39][40]), they are still at their infancy in the context of flood hazard.

In this paper, the scour problem is examined from the point of view of bridge response and relevant potential structural damage. To this aim, a multi-span masonry arch bridge, representative of many bridges built in Europe, is considered as case study, and extensive numerical analyses are performed to select a set of global kinematic parameters that are significantly affected by the scour and that are directly related to the bridge damage, (e.g., displacements and rotations on piers, spandrels and arches, twist at deck level, vertical settlements, natural frequencies and mode shapes). The failure mechanisms and damage states developed during the scour process evolution are analysed by considering two scour scenarios: a local one, involving a single pier, and a global one, involving all piers simultaneously.

The study results allow identifying parameters that are easily monitorable (e.g. by total stations, lidars, tilt-meters, and so on) as well as sensitive to scour, in order to use them as damage metrics for quantifying the effects of scour on masonry arch bridges. The relationships between the scour metrics and the proposed damage metrics are also evaluated, and these information allow to pursue monitoring strategies in which the effects of the scour are only measured and, indirectly, information upon the developed scour level is also available, without the need of directly investigating the cause (e.g., via scour probes, sonar devices, etc.). The outcomes also provide useful information for guiding the definition of optimal monitoring strategies and adequate sensor specifications (e.g. in terms of required accuracy, resolution and precision).

Moreover, the definition of suitable scour damage metrics is also useful for informing the development of probabilistic frameworks for the performance-based assessment of masonry arch bridges exposed to scour, where proper engineering demand parameters (EDPs) must be considered to develop fragility functions.

Damage metrics for masonry bridges under scour scenarios

Besides kinematic parameters, also parameters related to the dynamic response (modal parameters) are considered, as they could be inferred by performing, e.g., operational modal analysis using recordings from accelerometers. For this reason the sensitivity of natural frequencies and modal shapes to scour is also assessed.

The paper is structured as follows. Section 2 provides an overview on failure mechanisms observed in real masonry arch bridges; Section 3 presents the selected case study, together with a detailed description of the numerical modelling strategy; the most sensitive response parameters stemming from numerical analysis are introduced in Section 4, where general criteria for the damage states definition are provided. Section 5 illustrates the results of the numerical simulations. In Section 5.1, the damage evolution and the damage states identified for two scour scenarios are presented, whereas in Section 5.2 the sensitivity to scour of the selected kinematic response parameters is assessed. Section 5.3 illustrates the sensitivity of the modal parameters. In Section 5.4, some recommendations are given on the optimal monitoring strategy for masonry arch bridges exposed to scour. The paper ends with a conclusion section where future researches are also outlined.

2. MASONRY BRIDGE FAILURE MECHANISMS

Masonry arch bridges are constituted by various structural components interacting with each other, namely the piers, the arches, the spandrel walls, and the infill. Depending on the severity of scour, the failure mechanisms observed in this bridge typology can affect one or more components with different levels of damage, as shown by the several collapses occurred in the past. The most recurrent failure modes observed when local scour undermines bridge piers are those identified in Figure 1, portraying the post failure state of four different bridges in Europe. The detected damage mechanisms are three, each involving a different structural component but all visible in each figure from (a) to (c).

These are:

Damage metrics for masonry bridges under scour scenarios

- 1) pier vertical settlement and upstream rotation. This is one of the first mechanisms to emerge, which evolves until quasi-vertical fractures open in the downstream part of the pier (the detached upstream part of the pier remains tilted upstream);
- 2) longitudinal and/or diagonal cracks on both arches adjacent to the pier exposed to scour, which represents one of the last mechanisms to develop, after which (full or partial) collapse of the bridge spans occurs;
- 3) upstream spandrel walls collapse, which could either occur as an independent mechanism at the early stages of the scour process, or it could be induced by the collapse of the other components.

It is worth to note that the failure mechanisms will be further discussed in Section 4, where the outcomes of the numerical simulations will be analysed in detail. It is also important to stress that multispan bridges are prone to progressive collapses, and under very intense floods the excavation underneath the piers can induce the collapse of multiple spans. This is the case, for instance, of Rubbianello bridge. Figure 1-d shows the post-flood event scenario for this bridge: the pier is rigidly rotated toward the upstream side and the adjacent spans are fully collapsed.

The observation of the above-presented failure mechanisms suggests that various global kinematic parameters can be selected as potential descriptors of the effects of scour on masonry arch bridges. In the following section, suitable parameters will be selected based on numerical analyses of a representative masonry arch bridge, and their sensitivity to the different global mechanisms that can be activated by typical scour scenarios will be evaluated, by taking into account that they should be easily monitorable, e.g. by total stations, lidars, tilt-meters, accelerometers.

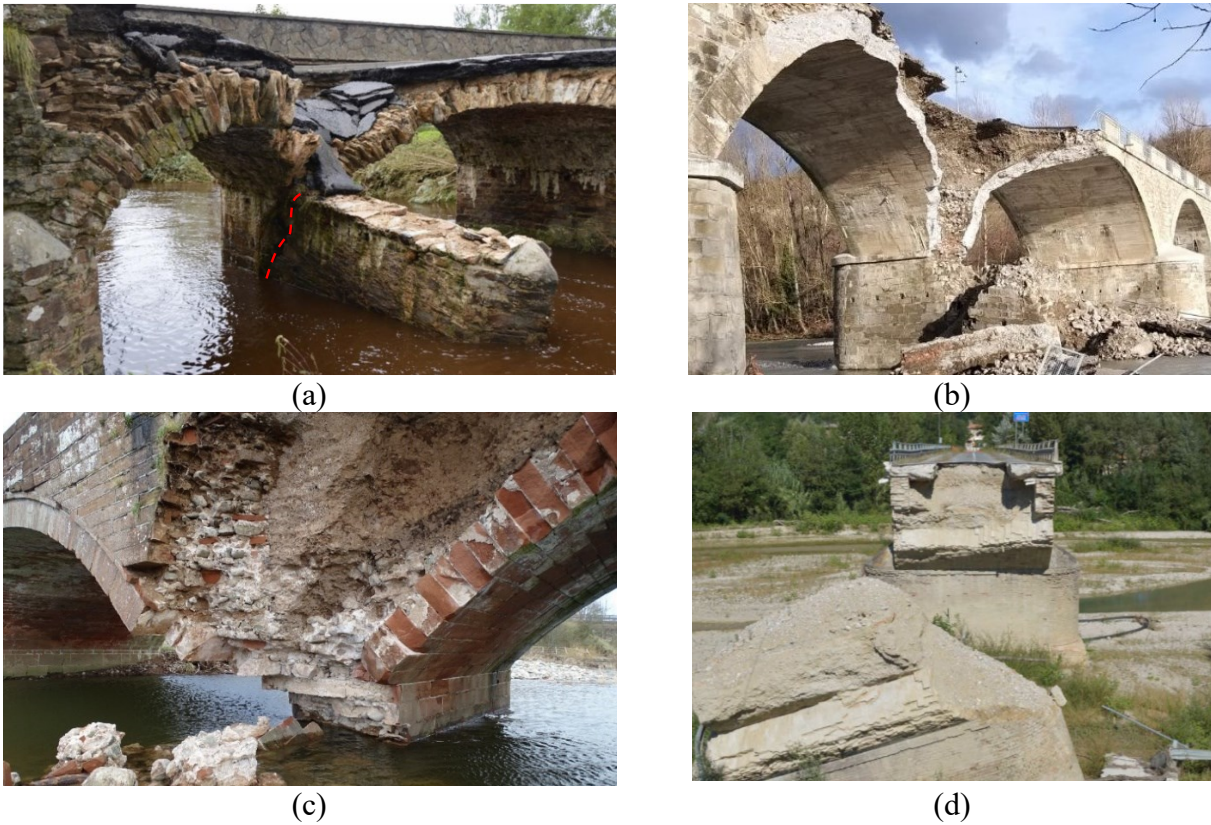


Figure 1. Examples of masonry arch bridge failure mechanisms. View from the upstream of: (a) Ballynameen Bridge over the River Faughn, Northern Ireland (photo courtesy of Gareth Scullion); (b) Samone Bridge on Panaro River, Italy (photo courtesy of lapressa.it); (c) Brougham Old bridge. (d) Lateral view of the collapsed Rubbianello bridge on Aso River, Italy.

3. NUMERICAL ANALYSIS

3.1 CASE STUDY

Masonry arch bridges are characterized by recurring geometrical features, with many existing bridges that are very similar to each other, as those shown in Figure 2. A bridge typology representative of the existing European bridge stock but also diffused worldwide is thus considered in this study, with geometry and features taken from a real bridge collapsed for scour in 2015 [18]. It consists of three spans 16.00 m long, for a total bridge length of 54.40 m (from abutment to abutment). The two piers are identical, with a plan size of 9.5 m x 3.2 m, excluding the extreme semi-circular cutwaters of 2.0 m radius; the segmental arches have thickness of 0.95 m and a radius of 11.58 m; the masonry

Damage metrics for masonry bridges under scour scenarios

spandrel walls have thickness of 0.65 m; the pier foundations have a rectangular plan shape of 11.00 m x 3.90 m and their height is 4.17 m. Figure 3 shows the longitudinal view of the bridge, together with the transversal and longitudinal sections.

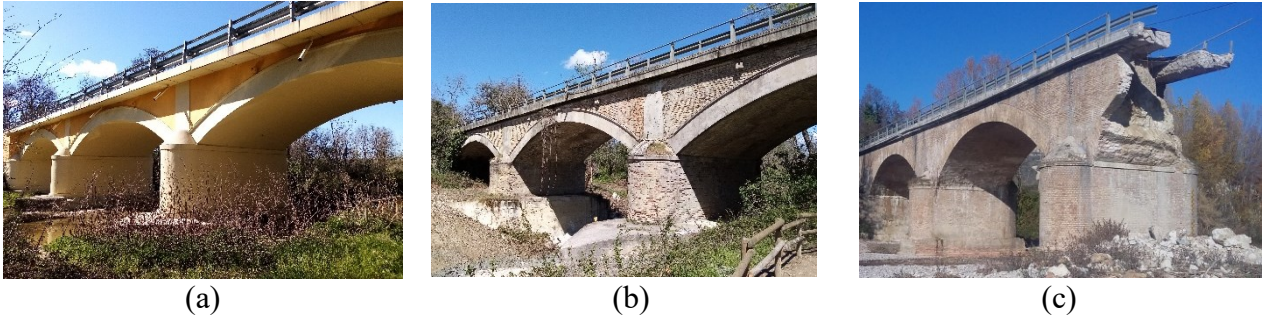


Figure 2. Examples of masonry arch bridges in Marche Region (Italy). In (c) the Rubbianello Bridge after flood-induced collapse in 2015.

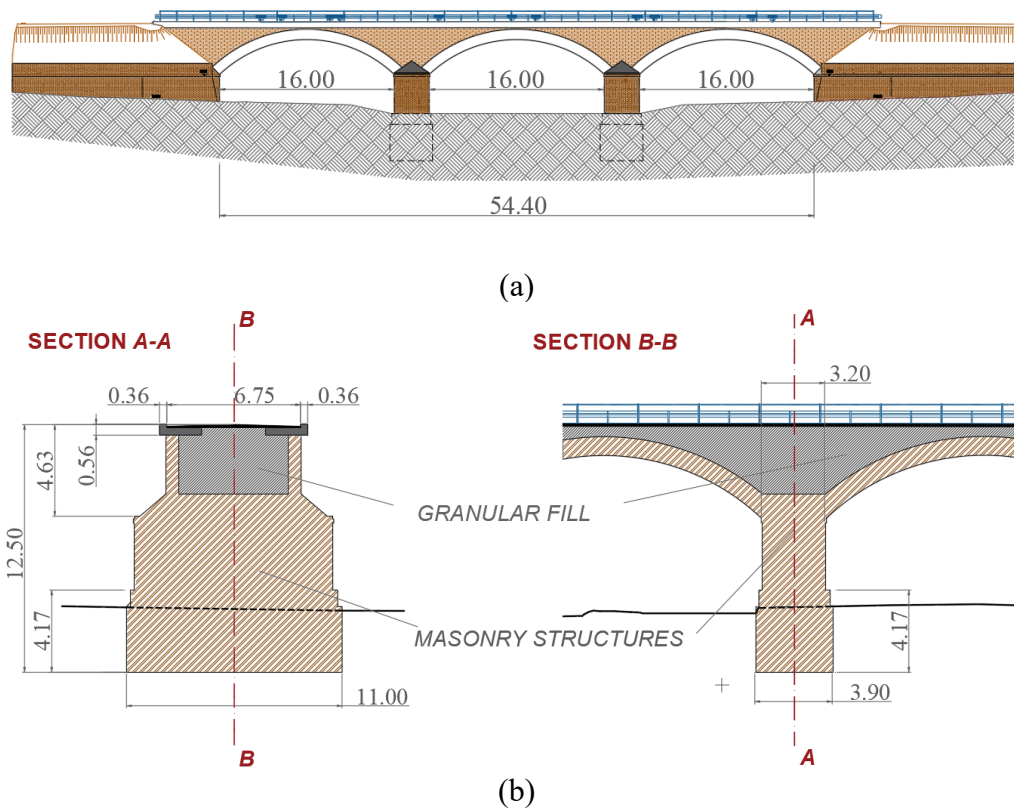


Figure 3. Scheme of the case study: (a) bridge longitudinal view, (b) transversal and longitudinal sections.

3.2 STRUCTURAL MODEL

A 3D model is developed in ABAQUS 2017 [41], by following the strategy adopted in [18] and here briefly recalled. The bridge model is built by using continuum solid elements with cohesive interfaces between the various components, and accounts for both geometrical and mechanical nonlinearities. The bridge components are discretised using linear hexahedral 8-nodes elements of type C3D8R, with 6 degrees of freedom per node. Parts with complex shapes are previously cut into simpler and more regular shapes in order to ease the mesh discretisation, which is performed using element with size variable between 0.2 m and 0.75 m in order to guarantee a good trade-off between results accuracy and computational cost. Coarser meshes are used for the master parts in defining contact pairs, to avoid compenetrating elements at the interfaces.

The elastic material properties of the different structural parts are summarised in Table 1.

For what concerns the non-linear behaviour, the adopted constitutive laws are as follows:

- masonry components are described using the Concrete Damage Plasticity (CDP) model [18], with plastic-strain – strength softening relationship as in Figure 4 (yielding compressive strength 1100 kN/m², maximum compressive strength 3850 kN/m², maximum/yielding tensile strength 150 kN/m²);
- granular fill material is linear elastic with a Mohr-Coulomb failure criterion characterized by a friction angle of 55° and a cohesion of 10 kN/m².

The following interfaces are used to simulate the interactions among the various bridge components:

- between the granular fill and any other bridge components, a frictional interface (friction coefficient of 0.60) is used along the tangential direction, and a “hard-contact” one along the normal direction (traction separation is allowed but parts in contact cannot compenetrates);

- mortar joints between walls and arches/piers and between arches and piers are modelled as both frictional (with a friction coefficient equal to 1.0) and cohesive interfaces, the latter assuming (according to [17]) normal stiffness $K_n = 0.4 \cdot 10^9 \text{ kN/m}^3$, tangential stiffness $K_t = 0.174 \cdot 10^9 \text{ kN/m}^3$, and tensile strength 150 kN/m^2 .

To improve numerical convergence, a damage stabilization criterion with viscous coefficient of 10^{-5} kNs/m is introduced. All the model parameters were assumed based on both in-situ and laboratory tests carried out in [18], with the only exception of the parameters characterising the interaction models, which were instead assumed consistently with the existing literature [17][42].

Similarly to previous studies [17][18], a simplified Winkler modelling approach has been considered to describe the soil-structure interaction, with axial springs distributed along the 4 vertical faces and the base face of the foundation and acting in compression only. Figure 5 shows the finite element model of the bridge including the springs modelling the soil-structure interaction. Table 2 illustrates the values of the stiffness per unit area along the horizontal (X,Y) and vertical directions (Z), derived according to the impedance formulation of [43] and to the assumed soil properties, reported in Table 1.

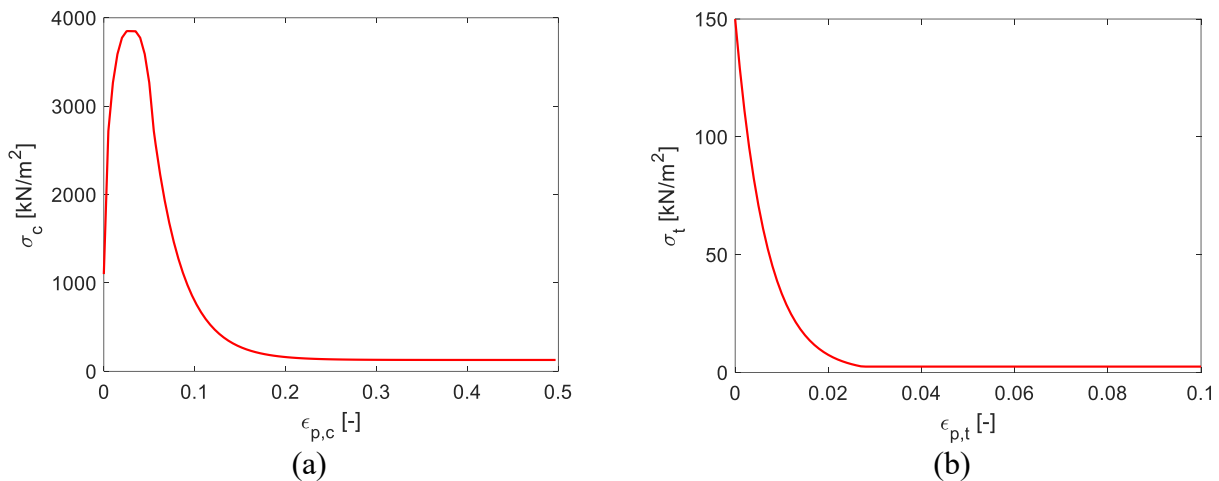


Figure 4. Masonry non-linear constitutive laws in compression and tension

Table 1. Material elastic properties.

Material [-]	ρ [t/m ³]	E [kN/m ²]	G [kN/m ²]	ϕ [°]
Masonry	1.80	3100000	-	-
Masonry (Piers only)	1.75	2900000	-	-
Backfill	1.70	250000	-	55
Abutment	1.90	300000	-	-
Soil	2.00	1065000	370000	38

Table 2. Elastic stiffness per unit area of the springs accounting for the soil-foundation interaction.

$K_{\text{soil},x}$ [kN/m ³]	$K_{\text{soil},y}$ [kN/m ³]	$K_{\text{soil},z}$ [kN/m ³]
220000	420000	940000

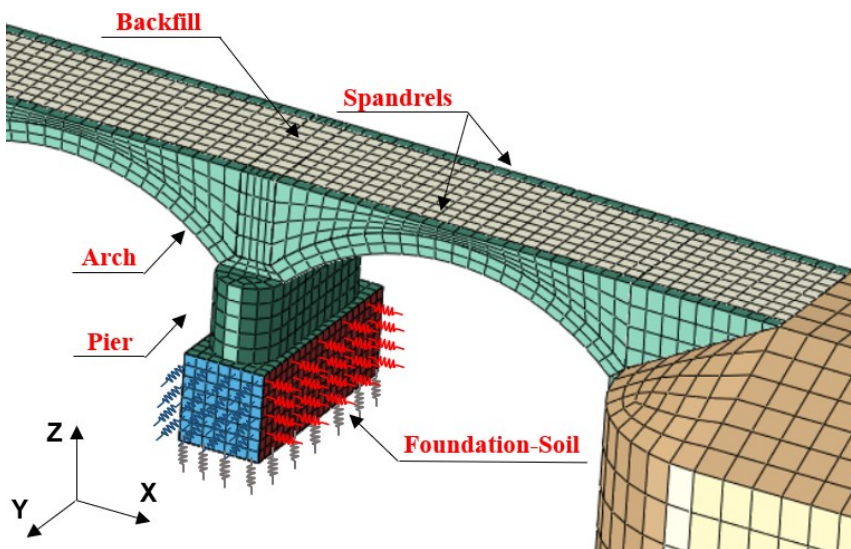


Figure 5. Finite element model, Winkler model of the soil-foundation, and global reference system.

3.3 SCOUR SIMULATION

Scour is simulated following the procedure outlined in previous works by the same authors of this study [17],[18], i.e., by progressively removing the springs that represent the reaction of the soil that surround the foundation. In particular, a pre-fixed, inverted pyramid shape is considered to describe the scour hole. This shape is a simplification of the scour hole geometry developing under ideal conditions in laboratory flume tests [1]. The geometry of the pyramid is defined entirely by the friction angle of the bed material φ , and by the maximum depth of scour y_s . The height coincides with the depth y_s , the upstream scour hole slope is assumed equal to φ , whereas the downstream slope is $\varphi/2$. Along the direction perpendicular to the flow, the scour hole shape is still triangular but with slopes equal to $5/6\varphi$, as evidenced by laboratory experimental tests conducted by other authors [44]. Reference can be made to Tubaldi et al. 2022 [11] for a more in-depth discussion about the scour hole shape. In [33], a numerical study conducted on a different system subjected to scour has shown that two scour hole shapes, characterised by a different geometry but the same value of B_s/B , induce similar effects in terms of changes of dynamic behaviour of the system.”

The progression of scour is simulated by considering increasing values of y_s and by removing the springs that are located into the scour hole. This approach allows to describe the two joint effects of scour, namely the loss of support and the settlements that consist in a translation and rotation at the pier base. This approach simulates a recurring mechanism of failure of masonry arch bridges, as previously discussed in Section 2. However, other scour scenarios may also take place, for example when the piers are not aligned with the flow, but such condition is not covered by the present study.

The simulated process is schematically illustrated in Figure 6, where two main parameters are adopted to quantify the level of evolution of the process: the ratio y_s/h (h being the height of the foundation, which coincides with the embedment level) and the ratio B_s/B (i.e., the ratio between the scoured width B_s and the total width B of the foundation). In fact, the effects of the scour start to become noticeable only for $y_s/h > 1$ or $B_s/B > 0$, i.e., when the base of the foundation starts to loose support, as also discussed in [45].

The numerical simulation of the scour process is achieved by performing a sequence of steps of static nonlinear analyses:

- the initial stage of analysis is carried out on the model without scour (i.e., all active boundary conditions represented by the horizontal and vertical soil-foundation springs) to apply the gravity loads (self-weight and a uniform pressure of 6.6 kN/m^2 accounting for the carried road pavement loads), which are then kept constant during the whole set of successive analyses;
- the following steps consist of gradually removing the springs from the foundation (of one or both piers depending on the scenario) simulating increments of the maximum scour depth from $y_s/h = 0.0$ ($B_s/B = 0$) to $y_s/h = 1.65$ ($B_s/B = 0.75$);
- the analysis terminates at $y_s/h = 1.65$, representing the condition after which the values of various response parameters start to increase in an uncontrolled manner for small increases of scour depth, and convergence issues also arise.

It is noteworthy that, in real cases, the portion of the piers immersed in the stream are subject to other concomitant actions, such as the uplift and drag forces. Their effects have been disregarded in this study for two reasons: it is expected they are not significant under typical conditions (see e.g., [46]), unless the water level is so high to reach the arch soffit and there are debris accumulated at the bridge; for typical values of the flow speed the entity of the drag forces is comparable to the entity of the wind forces, which are therefore negligible on massive structures such as masonry bridges.

Damage metrics for masonry bridges under scour scenarios

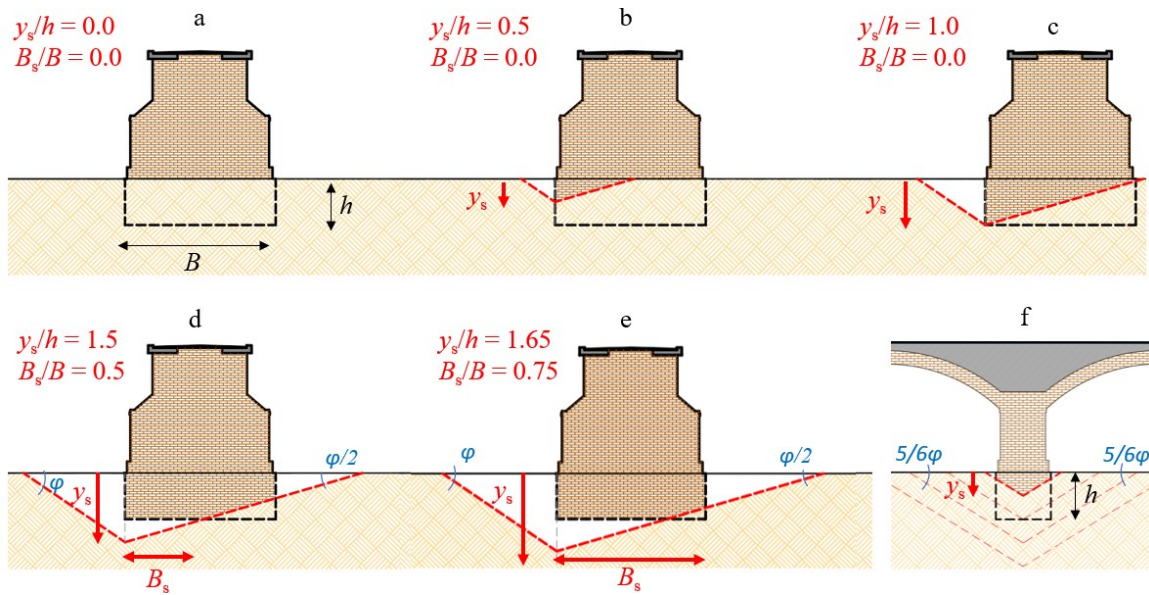


Figure 6. Illustration of the scour hole evolution and related parameters: a)-e) view parallel to the flow; f) view orthogonal to the flow.

4. KINEMATIC RESPONSE PARAMETERS AND DAMAGE LEVELS

Two alternative scour scenarios are considered: the first one (denoted as local scour scenario) represents the case of a flow impinging only on one pier, producing a localised scour. The second scenario (denoted as global scour scenario) is a more idealised case where the flow impinges with the same conditions on both piers, thus simulating a more diffused erosion which corresponds to a combination of global, contraction and local scour.

Numerical simulations are performed by considering both the local and global scour scenarios and by adopting the strategy described in the previous section. Based on the analysis results (see deformed shapes in Figure 7, referred to scour levels $B_s/B = 0.60$), a set of global kinematic response parameters is identified as potential descriptors of the effects of scour on the masonry arch bridge. More specifically, such parameters are selected based on these criteria: they must be sensitive to the scour progression and to the different damage mechanisms which are gradually activating, and they must also be monitorable, via traditional or less-common monitoring strategies (e.g. total stations, lidars, tilt-meters, satellite monitoring to name few).

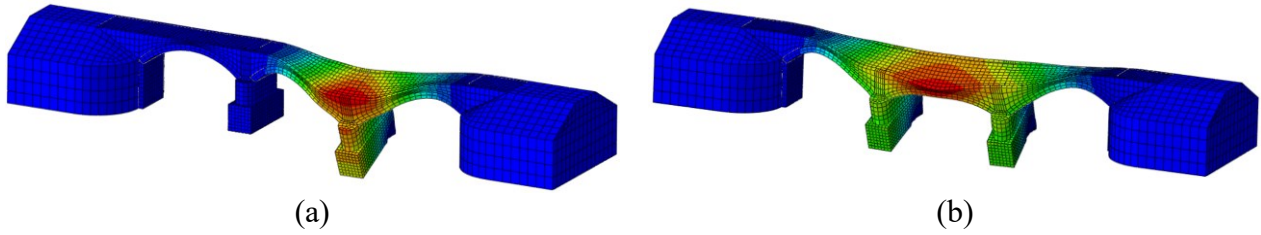


Figure 7. Bridges deformed shapes (10x amplified) for both (a) local and (b) global scour scenarios.

The kinematic parameters identified for each scour scenario, schematically represented in Figure 8, are: transversal and vertical displacements of selected structural points (u_z and u_y); rotations (θ) of piers, spandrels and arches, and twist at deck level; diagonal tension strains (ε) on decks and piers.

The level of sensitivity of these response parameters is assessed in Section 5, where the results from the numerical analysis are presented. The red dots shown in Figure 8 identify nodes whose displacements revealed to be not sensitive to the specific scour scenario (as can be seen from Figure 7) and thus they are excluded from the presentation of the results.

Once suitable response quantities are selected, threshold values can be identified to characterize the attainment of particular damage conditions on the bridge. To this aim, a set of damage states are identified based on the analysis of the damage evolution observed on bridge components. In particular, the following two quantities are considered:

- plastic strain increments on the structural elements;
- crack width w , indirectly estimated [47] by the product of the equivalent plastic strain in uniaxial tension ε^{pl} (experienced by the element at a given analysis increment t) and the size of the yielding element b :

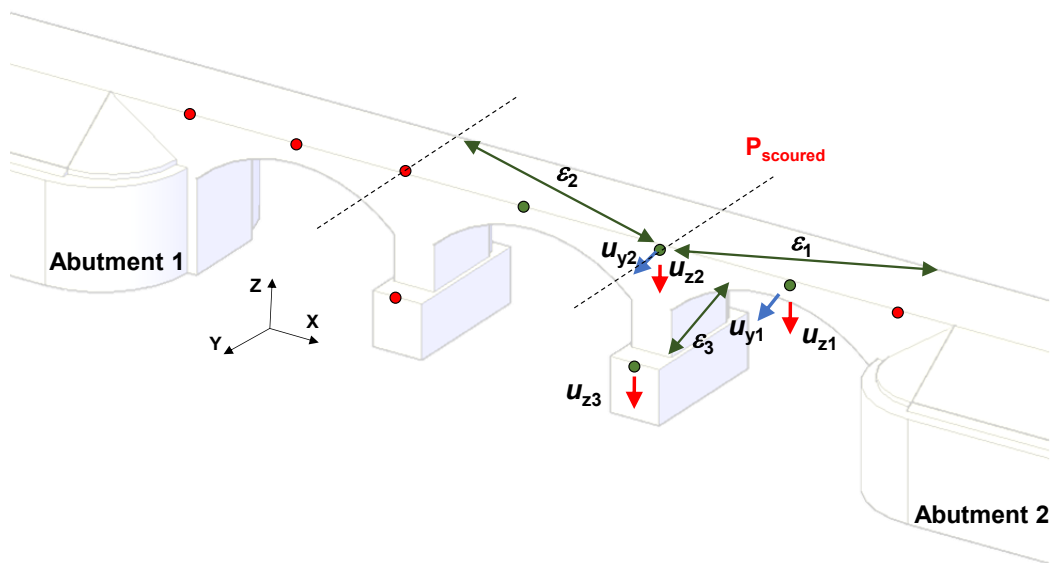
$$w(t) = b \cdot \int \varepsilon^{pl} dt \quad (1)$$

The following damage states are proposed:

Damage metrics for masonry bridges under scour scenarios

- Slight Damage (DS1): first plastic strains (both tension and compression) developing on minor structural components (e.g., spandrel walls) corresponding to the beginning of a kinematic mechanism;
- Severe damage (DS2): cracks starting to open on spandrel walls and piers;
- Near Collapse (DS3): spreading of damage on spandrel walls and piers and cracks formation on arches.

It must be noted that the damage mechanisms are different in the two scour scenarios, hence the damage states presented above should be viewed as qualitative, while a more detailed and quantitative discussion (with explicit identification of the corresponding scour levels) is provided when numerical results are presented.



(a)

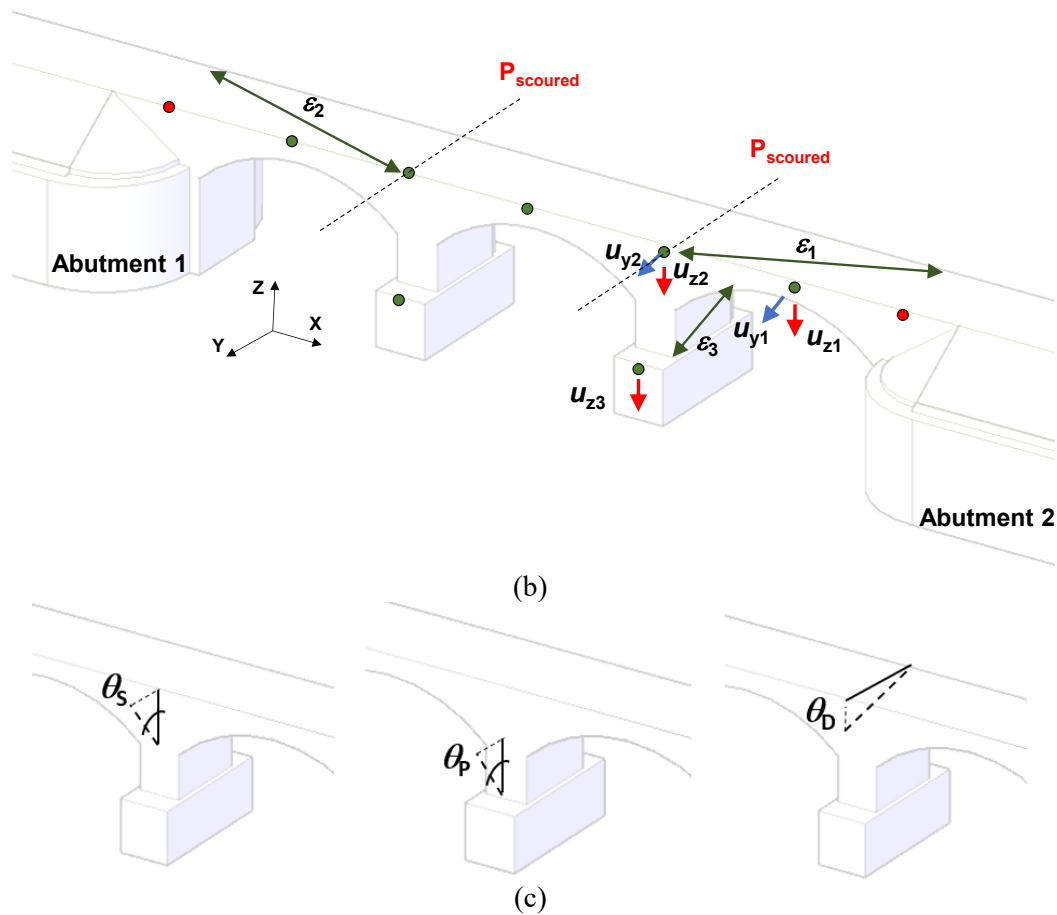


Figure 8. Scheme of the monitored kinematic parameters for the scour scenario involving (a) one pier only and (b) two adjacent piers. (c) structural components rotations (common for both scour scenarios): spandrel wall, pier and deck tilt.

5. NUMERICAL RESULTS

This section reports the results deriving from the numerical simulations. First, the damage states identified for the two scour scenarios are presented (Section 5.1), then the different selected response parameters are compared (Section 5.2) in order to assess their sensitivity with respect to the scour process evolution; finally, the sensitivity of the modal parameters to the scour evolution is evaluated (Section 5.3).

5.1 DAMAGE STATES

5.1.1 *Local scenario: scour localised under one pier*

Damage states are identified by observing the results of the analysis and by monitoring the damage evolution, according to the criteria described in Section 4. The identified damage states are shown in Figure 9, where each state is associated to the corresponding level of scour (described through the ratios y_s/h and B_s/B) and plots of the bridge model with highlighted the elements actively yielding at that step of analysis are provided. A description of the identified damage states is provided below:

- Slight Damage DS1 ($y_s/h = 1.28$, $B_s/B = 0.32$): first plastic strains developing on spandrel walls according to a pattern (upstream wall face on the scoured pier and downstream wall faces on the abutment and lateral pier), corresponding to the beginning of a kinematic mechanism; entity of tension cracks is negligible;
- Severe damage DS2 ($y_s/h = 1.39$, $B_s/B = 0.48$): piers start developing slight pseudo-vertical cracks of estimated width of 2-3 mm and spandrel walls damage increases (estimated crack width > 3 mm);
- Near Collapse DS3 ($y_s/h = 1.51$, $B_s/B = 0.62$): damage spreads all over the structural elements, diagonal cracks of few millimetres appear on arches, and immediately after the values of response parameters start to increase in an uncontrolled manner for small increases of the scour depth.

It should be noted that the adopted modelling strategy, due to its limitations (e.g., continuous model for describing masonry components, simplified Winkler approach for soil-structure interaction, idealised scour hole shape, etc.), can accurately capture the response of the bridge until the onset of the collapse mechanism. This limitation of the model is also at the base of the choice of defining a near-collapse condition. A more refined modelling strategy possibly based on discrete elements or applied element methods, would be needed to describe more accurately the collapse condition of the bridge.

Anyway, despite the limitations of the model, the identified failure mechanisms are in good agreement with the ones observed in real cases and presented in Figure 1, showing damage of spandrel walls, quasi-vertical fractures opening on piers, and diagonal cracks on arches adjacent to scoured pier.

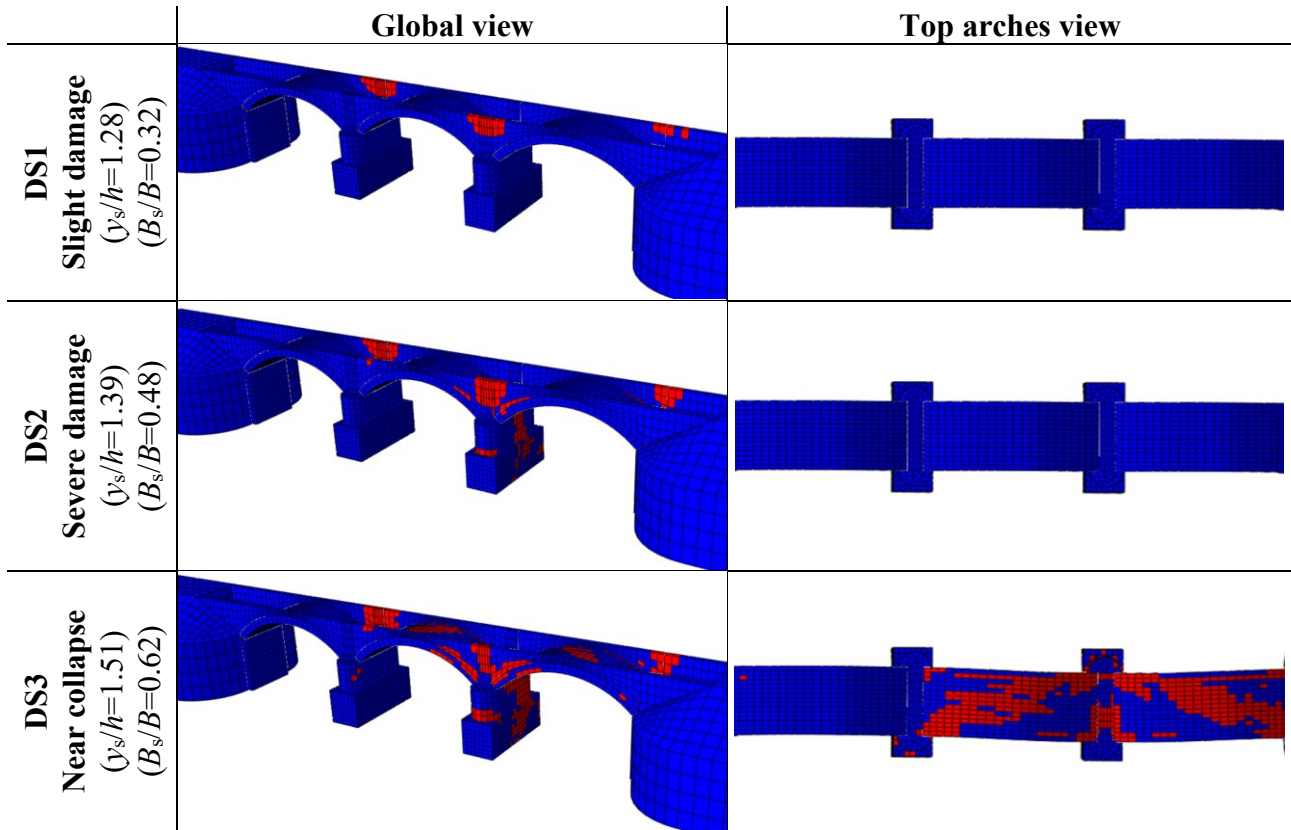


Figure 9. Damage states identified for the local scour scenario (elements currently yielding are highlighted in red).

5.1.2 Global scenario: scour under both piers

The damage states identified for the global scour scenario are presented in Figure 10, which highlights in red the elements currently yielding. The damage states can be described as follows:

- Slight Damage DS1 ($y_s/h = 1.25$, $B_s/B = 0.30$): first plastic strains developing in the two scoured piers and in the spandrel walls according to a pattern (upstream side of the scoured piers and

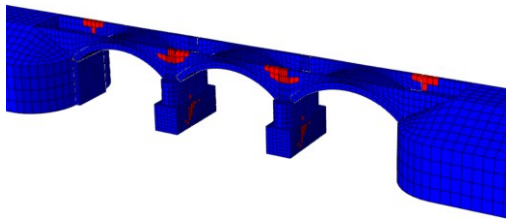

Damage metrics for masonry bridges under scour scenarios

downstream side of the abutments), corresponding to the beginning of a kinematic mechanism; entity of tension cracks is negligible;

- Severe damage DS2 ($y_s/h=1.35$, $B_s/B=0.41$): widespread damage in piers and spandrel walls and first diagonal cracks (<1mm) appearing on the side arches;
- Near Collapse DS3 ($y_s/h=1.43$, $B_s/B=0.52$): damage spreading all over the structural elements with estimated crack widths exceeding 10 mm; moreover, an horizontal arch mechanism develops within the central arch and the values of response parameters start to increase in an uncontrolled manner for small increases of the scour depth just right after.

According to the outcomes presented for both the scour scenarios, it can be observed that damage mechanism DS1 is triggered for values of B_s/B of around 30%, while the system failure is attained for levels of B_s/B higher than 50% -60%, depending on the type of scour (global or local). Such high levels of scour required to induce collapse of masonry arch bridges can be explained by the significant robustness of this bridge typology. In fact, it is not uncommon to find cases of bridge piers that are not collapsed even when half their base is scoured, and cases of bridge failure with the pier base excavated up to the 80% of its width.

For sake of clarity, the levels of scour activating the various damage states are summarised in Table 3 for both the scenarios: it can be observed how the damage evolution is faster in the case of global scour scenario; the limit states, indeed, are attained for levels of excavation slightly lower than those corresponding to the local scour scenario.

	Global view	Top arches view
DS1 Slight damage $(y_s/h=1.25)$ $(B_s/B=0.30)$		

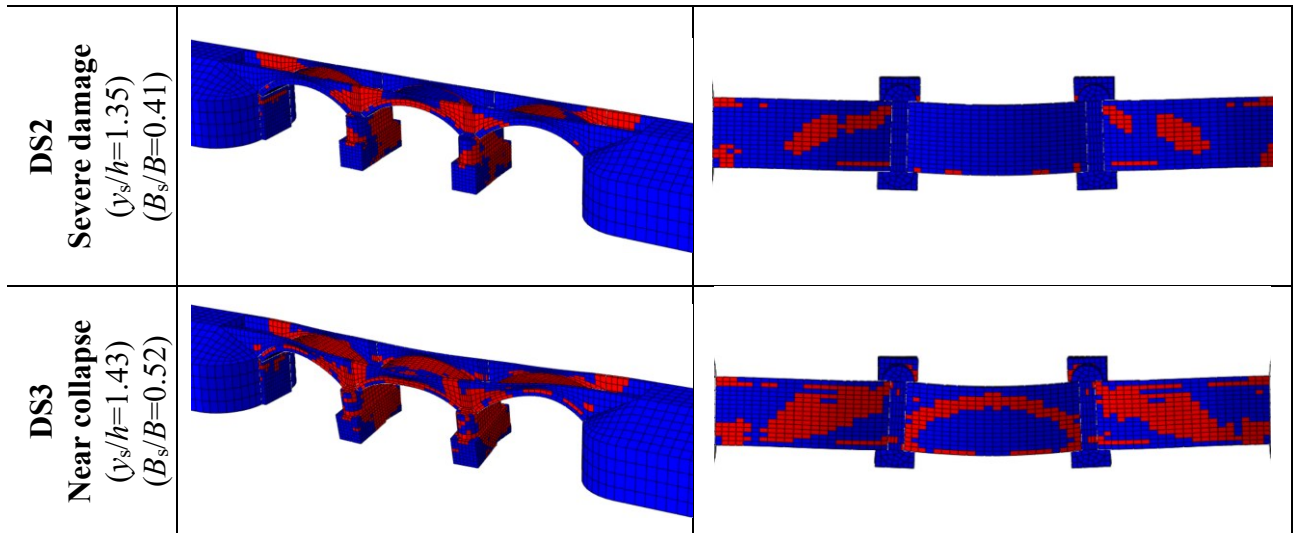


Figure 10. Damage states identified for the global scour scenario (elements currently yielding are highlighted in red).

Table 3. Levels of scour (y_s/h and B_s/B) at which the damage states are attained.

Damage States	Local scour		Global scour	
	y_s/h	B_s/B	y_s/h	B_s/B
DS1 Slight damage	1.28	0.32	1.25	0.30
DS2 Severe damage	1.39	0.48	1.35	0.41
DS3 Near collapse	1.50	0.60	1.43	0.52

5.2 KINEMATIC RESPONSE PARAMETERS

To assess the suitability of the response descriptors, the selected response parameters are now examined by looking at: 1) the gradient of growth with the scour progression, which is directly related

to the parameter's sensitivity and should be as high as possible for the response descriptor to be sensitive to scour; 2) the presence of a monotonic trend, which is necessary for correctly identifying the level of scour.

Besides the comparison of the physical quantities, a normalized comparison is also presented in order to eliminate the effects related to the different scale and nature of the considered measures. For this purpose, each parameter D is normalized by the relevant response value D_{DS3} attained for the near collapse damage state, according to the following expression:

$$D_N = \frac{(D - D_0)}{(D_{DS3} - D_0)} \quad (2)$$

where D_0 denotes the response value before the scour process initiation.

In the next subsections the results are presented separately for the two considered scour scenarios and the most suitable response parameters are identified; then, the most sensitive parameters found from each scenario are also compared.

5.2.1 Local scour scenario

The response quantities of interest could be plotted as a function of the one of the two independent variables (y_s/h or B_s/B) previously introduced to describe the scour intensity. For example, Figure 11 illustrates the variation of the pier vertical settlement with y_s/h (Figure 11a) and with B_s/B (Figure 11b). The second type of representation is more effective and will be used hereinafter because it better characterizes the process, given that no significant effects occur on the bridge for scour levels lower than the foundation height ($y_s/h < 1.0$ or $B_s/B=0$). Moreover, in each figure the three identified damage states are highlighted through vertical light grey dotted lines.

Damage metrics for masonry bridges under scour scenarios

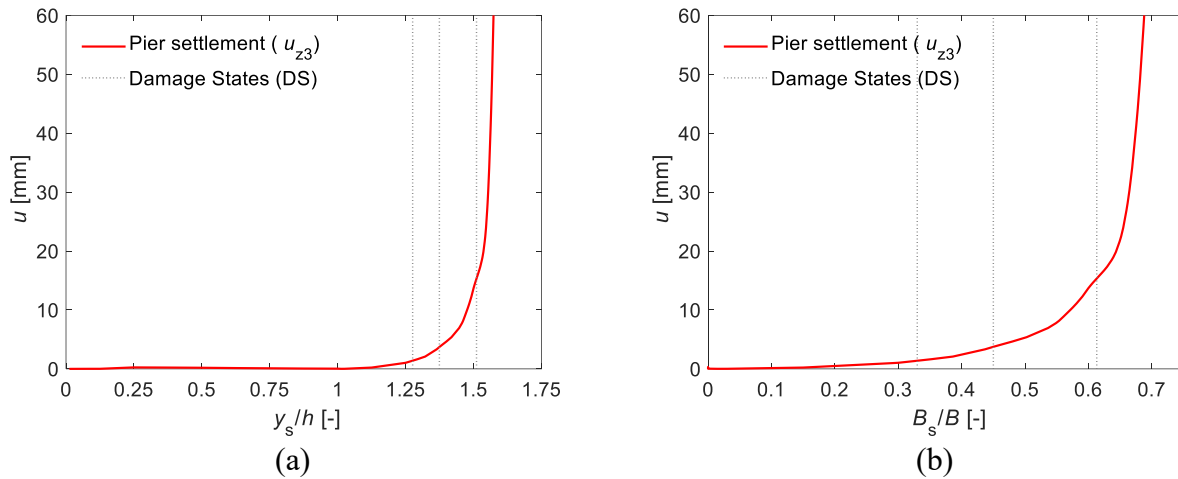


Figure 11. Plot of the same response parameter (pier vertical settlement) as a function of two different scour progression parameters. i.e., the ratios (a) y_s/h and b) B_s/B .

Figure 12 illustrates the variation of the monitored response parameters as a function of the ratio B_s/B . Figure 12a-b compares the various displacement measures, Figure 12c-d the strain measures, and Figure 12e-f the rotation measures. The left figures show the quantities with their physical units, whereas the right figures show the measures normalised according to Eq (2). The following observations can be made:

- all the considered response parameters increase at a significant rate after the near-collapse damage state is attained, suggesting that the bridge is close to collapse.
- the various displacement measures (both vertical and transversal) exhibit similar trends, also in the normalised plots (Figure 12b), with curves almost superimposed and comparable slopes, meaning that these selected metrics are all suitable and equivalent in detecting the effects of scour on the structure.
- the two considered strain measures (Figure 12c-d) show different trends. While the deck strain measure is a good and sensitive metric, the pier strain measure has the shortcoming of following a non-monotonic pattern. This is due to the evolving mechanism at the base of the pier, characterised by a variable centre of rotation which gradually moves from the upstream toward the downstream of the basement. Thus, it is not suitable for tracking the increase of scour.

Damage metrics for masonry bridges under scour scenarios

- the three investigated rotation measures (Figure 12e-f) are all suitable with similar sensitivity to the scour.

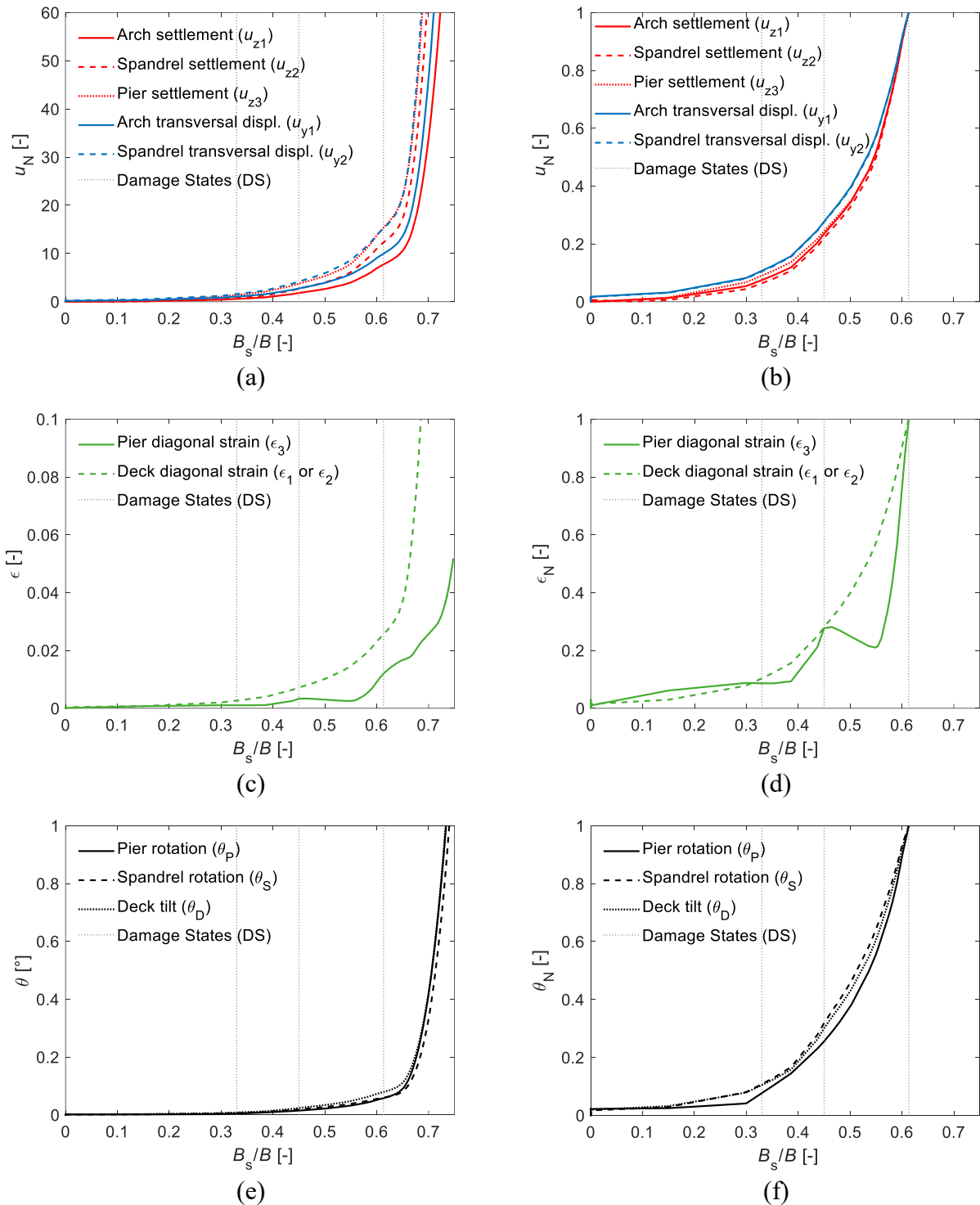


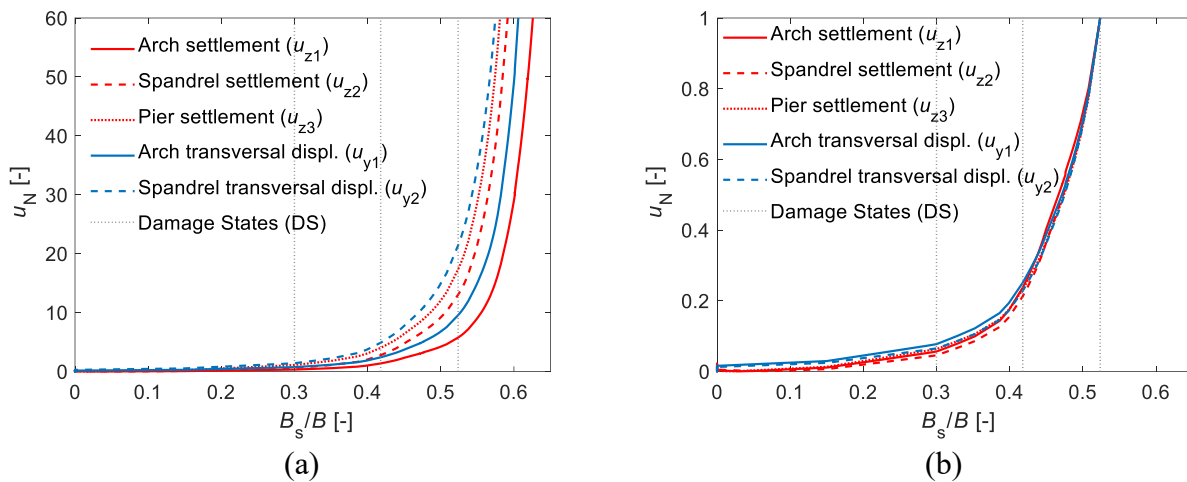
Figure 12. Local scour scenario (excavation under single pier). Sensitivity of different kinematic response parameters to the scour evolution described through the parameter B_s/B : (a) not normalized and (b)

Damage metrics for masonry bridges under scour scenarios

normalized (vertical and transversal) displacements; (c) not normalized and (d) normalized pier's and deck's strains; (e) not normalized and (f) normalized pier/spandrel rotations and deck tilt.

5.2.2 Global scour scenario: excavation under both piers

Figure 13 shows the monitored response parameters as a function of the ratio B_s/B . The comments made for the first scenario apply to these outcomes as well, with the only difference related to the scour levels at which the mechanisms (thus the curves) change. Indeed, it is observed that the curves corresponding to the global scenario start increasing earlier than those corresponding to the local scour scenario, as can be better appreciated from Figure 14, where the direct comparison between the two scenarios is made in terms of one of the most sensitive response parameters (i.e., the spandrel wall transversal displacement). Coherently, as already pointed out in Section 5.1, the damage states (plotted with vertical coloured dotted lines) of the global scour scenario are slightly anticipated compared to those of the local scour scenario.



Damage metrics for masonry bridges under scour scenarios

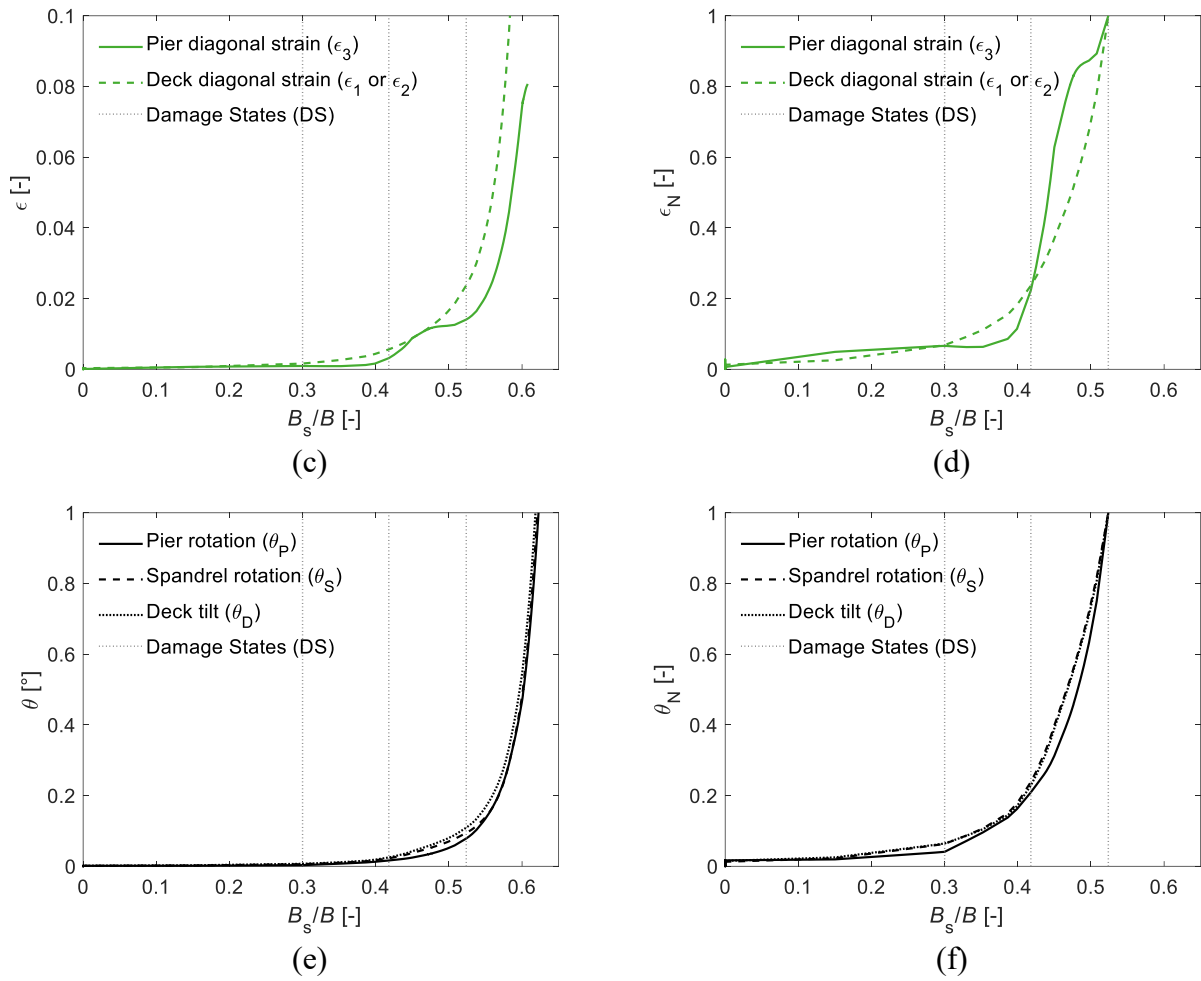


Figure 13. Global scour scenario (excavation under single pier). Sensitivity of different kinematic response parameters to the scour evolution described through the parameter B_s/B : (a) not normalized and (b) normalized (vertical and transversal) displacements; (c) not normalized and (d) normalized pier's and deck's strains; (e) not normalized and (f) normalized pier/spandrel rotations and deck tilt.

Damage metrics for masonry bridges under scour scenarios

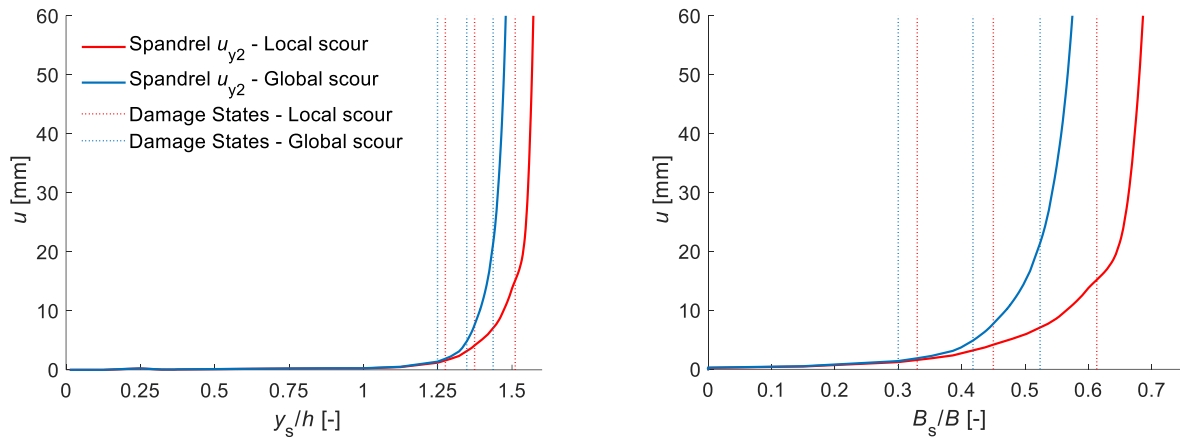


Figure 14. Comparison between local and global scour scenarios: scour progression described (equivalently) by the ratio (a) y_s/h and b) B_s/B .

5.3 MODAL RESPONSE PARAMETERS

In addition to the analysis of the response in terms of kinematic parameters, the influence of the scour progression on the modal properties is assessed in this subsection. For this purpose, an eigenvalue analysis has been carried out in Abaqus at the end of each step where the scour depth increment has been applied, in order to evaluate the variation of the modal properties due to scour and related effects. Figure 15 illustrates the effect of scour levels of increasing intensity on the transverse mode shape, for both the analysed scenarios (local scour on the left and global scour on the right). It can be observed that the mode shape variation is not significant in the case of global scour, whereas important changes occur in the local scour scenario. In the latter case, it is worth noting how such change in modal shape can be appreciated even before the foundation base starts being excavated,

Damage metrics for masonry bridges under scour scenarios

i.e., for $y_s/h > 0.75$ (when B_s/B is still zero). On the contrary, mode shape changes in the global scour scenario start to be (slightly) visible for $y_s/h > 1.25$ only.

Regarding the influence of the scour on the natural frequencies, Table 4 collects both the frequencies and the percent variations, $\Delta f_{\%}$ (with respect to the reference, no scour, value), observed at different levels of excavation:

$$\Delta f_{\%} = 100 \frac{(f_0 - f)}{f_0} \quad (3)$$

where f_0 is the reference initial natural frequency of the bridge and f is current frequency value.

Moreover, a normalised measure of the natural frequency variation, Δf_N , is introduced according to the following expression:

$$\Delta f_N = \frac{(f_0 - f)}{(f_0 - f_{DS3})} \quad (4)$$

where f_{DS3} is the frequency corresponding at the near collapse damage state.

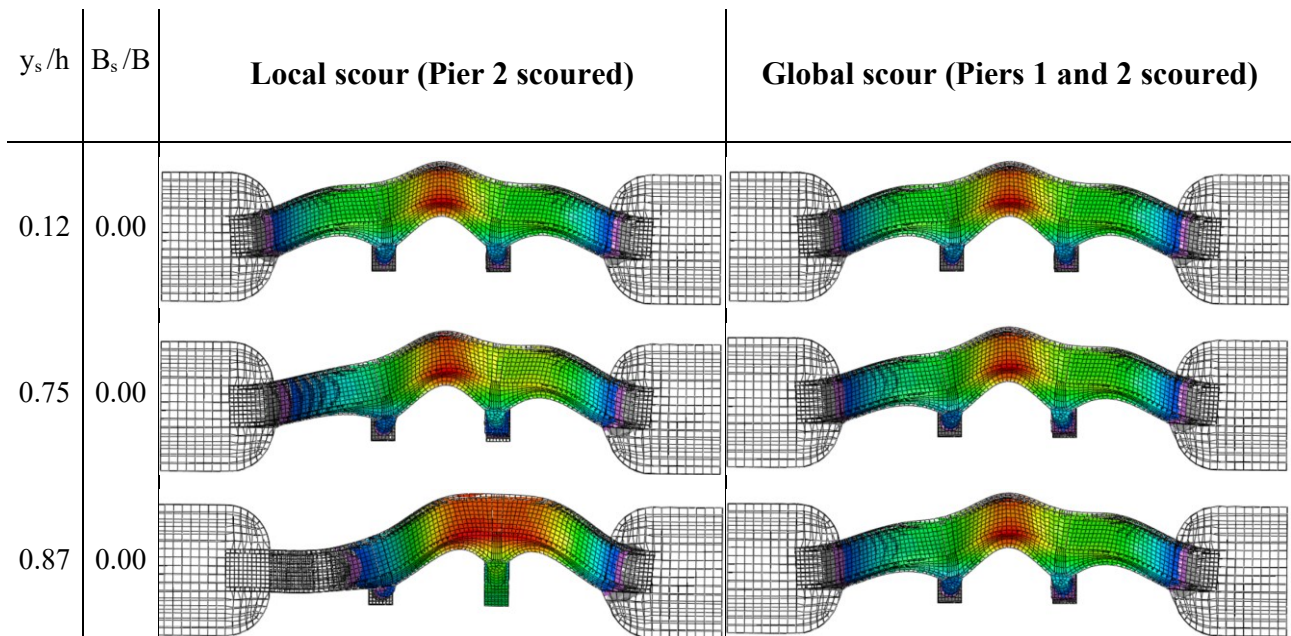
A plot of both the percent and normalised variation of the frequencies over the scour levels are provided in Figure 16 (scour evolution described by the ratio y_s/h) and in Figure 17 (scour evolution described by the ratio B_s/B).

The main conclusions stemming from these results are as follows:

- frequency percent variation (in absolute value) are slightly higher when a single pier is scoured, rather than both piers scoured;
- significant frequency modification are only observed for scour levels $y_s/h > 1.00$, and this can be better appreciated from the plots of Figure 17a (e.g., the initial vertical branch of the curves attains values lower than 5.0% while $B_s/B = 0.0$);
- frequency variations higher than 14% only occur for $y_s/h > 1.25$ (i.e., for $B_s/B > 0.28$);

- the normalised frequency variations for the two scour scenarios are almost perfectly superimposed, and this demonstrates that their sensitivity to scour is very similar.

A few comments are warranted concerning the usage of these results in real applications, i.e., when modal identification techniques under ambient noise are adopted. In these cases, the acceleration measurements might be affected by several aspects, including the sensor self-noise, or humidity levels and temperature. These latter are recognised to have an impact on the estimate of the natural frequency values, with relative variations which are usually below 5.0% [48]. This would mean that frequency reductions induced by scour levels lower than the foundation depth (i.e., $y_s/h < 1.0$) could easily be obscured by the environmental effects. Under these circumstances, it may still be possible to exploit the mode-shape variation as scour identification method, given the higher sensitivity to scour and the fact that environmental conditions generally do not alter the estimates of the vibration mode shapes [48][49].



Damage metrics for masonry bridges under scour scenarios

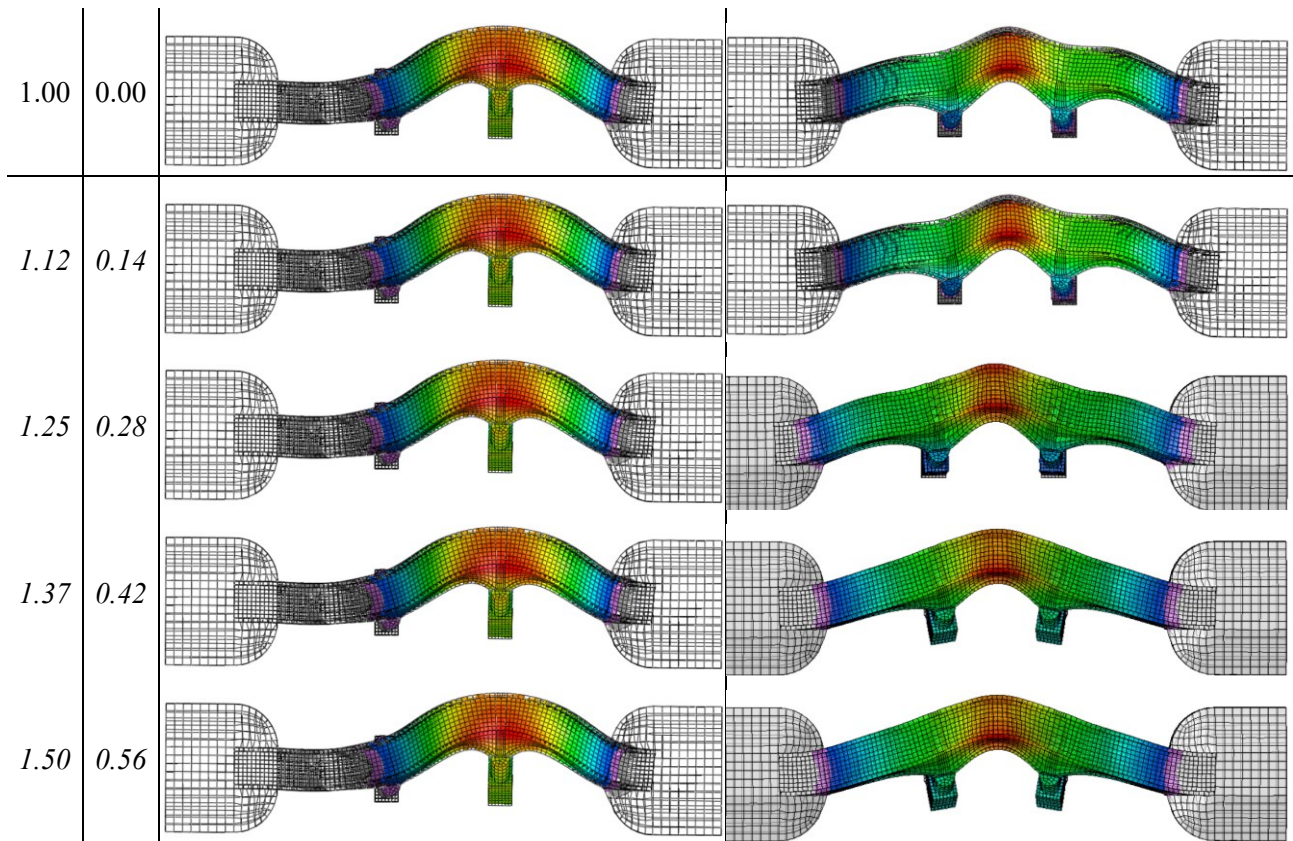


Figure 15. Effect of scour levels of increasing intensity on the transverse mode shape, for both the analysed scenarios (local scour on the left and global scour on the right).

Table 4. Modal frequency evolution at different scour levels: absolute values (Hz) and % variation.

		0.00	0.12	0.25	0.37	0.50	0.62	0.75	0.87	1.00	1.12	1.25	1.37	1.50
		0.00	0.00	0.00	0.00	0.00	0.00	0.00	0.00	0.00	0.14	0.28	0.42	0.56
Local scour	f [Hz]	6.48	6.48	6.48	6.48	6.43	6.37	6.31	6.23	6.14	5.84	5.21	4.30	-
	Δf [%]	0.00	0.00	0.00	0.00	0.77	1.70	2.62	3.86	5.25	9.88	19.60	33.64	-
Global scour	f [Hz]	6.48	6.48	6.48	6.48	6.47	6.43	6.38	6.32	6.27	6.04	5.56	4.82	3.95

Δf [%]	0.00	0.00	0.00	0.00	0.15	0.77	1.54	2.47	3.24	6.79	14.20	25.62	39.04
----------------	------	------	------	------	------	------	------	------	------	------	-------	-------	-------

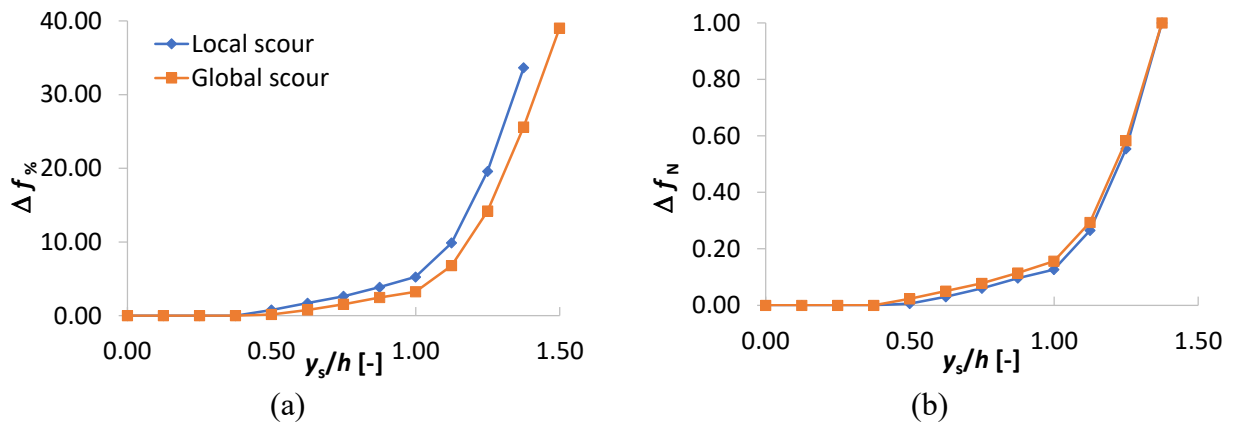


Figure 16. Natural frequency variations as a function of the scour ratio y_s/h : (a) percent variations and (b) normalized variations.

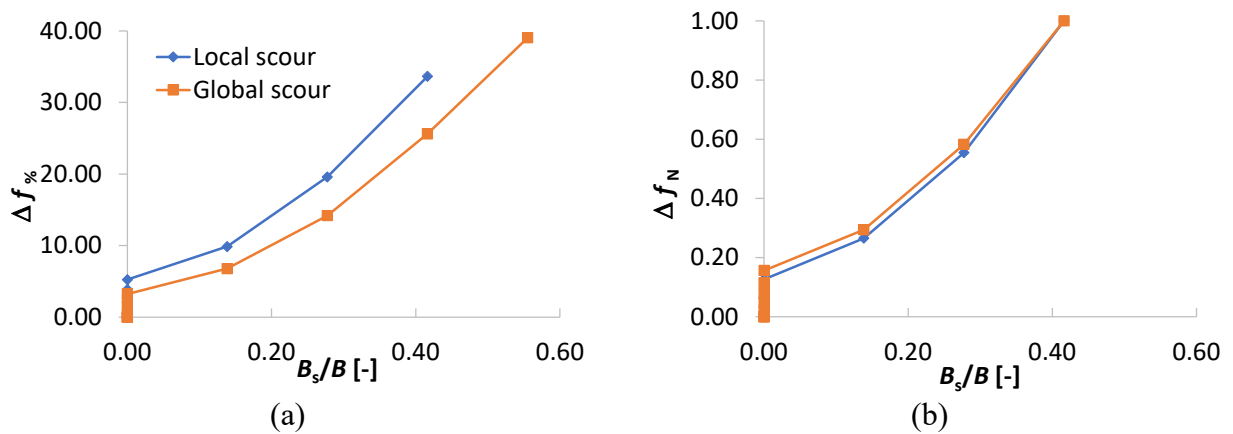


Figure 17. Natural frequency variations as a function of the pier basement excavation ratio B_s/B : (a) percent variations and (b) normalized variations.

5.4 OPTIMAL MONITORING STRATEGY

The results reported in the previous subsections can be exploited to suggest possible monitoring strategies to be implemented within long-term campaigns aimed at detecting the scour evolution underneath one or more piers. According to the response sensitivity analysis results, the parameters

illustrated in Figure 18 and listed below could be monitored (for each physical quantity to be measured, one or more potentially suitable strategies/sensors are proposed):

- Diagonal relative displacements/strains along the surface of the deck (according to the configuration of Figure 18, see green dashed arrows). These could be measured for example using fiber optic sensors, total stations, or satellite-based differential interferometry (InSAR) [50].
- Out of plain pier rotations, which could easily be monitored via tiltmeters [51] located at the upstream side of the piers.
- Transversal accelerations, measurable through accelerometers (also just unidirectional along Y) placed according to two possible configurations: in correspondence of the piers only, or in correspondence of the piers and in the middle of each span. The first configuration represents a minimum requirement in order to reconstruct the modal features of interest, the second yields a better resolution of the modal shape estimate.
- Finally, a vision-based monitoring strategy [52] could be used as a possible supplementary (low cost) technique, with high resolution cameras installed at suitable locations upstream of the bridge, exploiting digital image correlation analysis. Further investigations are required to verify that the resolution of the derived data can be sufficient for the purpose.

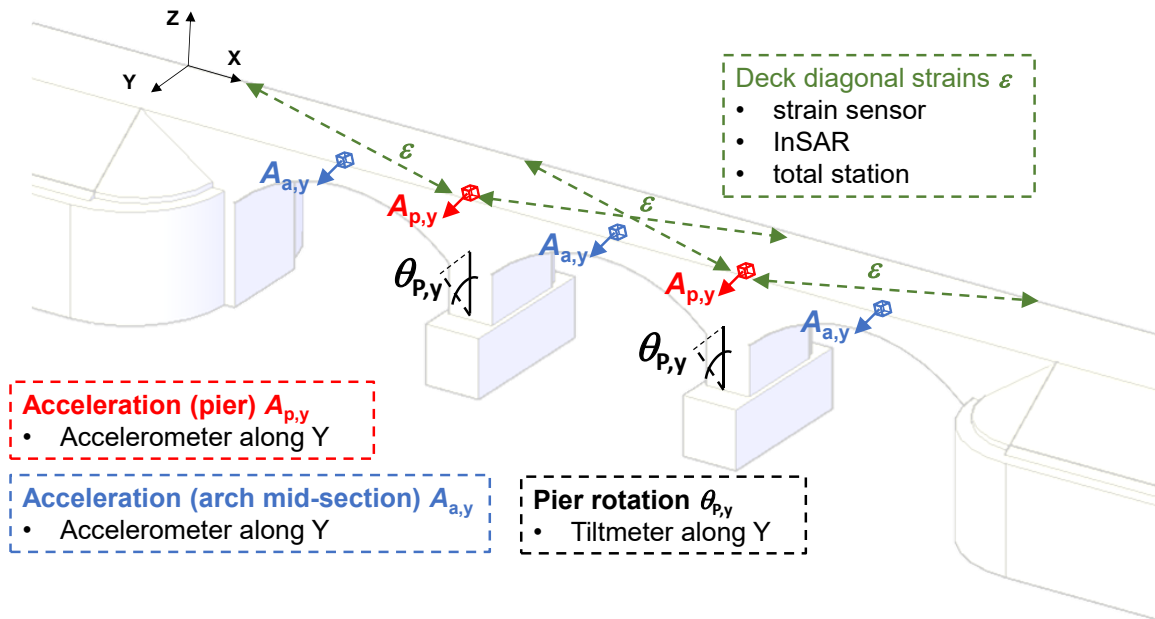


Figure 18. Scheme of the minimum optimal sensors setup to be implemented within a long-term monitoring campaign aimed at detecting the scour evolution under the bridge.

It is noteworthy that the noise produced by the environmental and operational conditions could hide the changes in the metrics considered to detect scour at the early stages of scour development. For example, Borlenghi et al. [51] has shown that temperature variations have an effect on pier rotations measurements in masonry arch bridges, whereas water elevation does not show any correlation with pier rotations. However, most of these effects can be compensated using proper algorithms trained on a sufficiently long period of observation.

6. CONCLUSIONS

In this paper, the impact of scour on masonry arch bridges has been thoroughly investigated. Extensive numerical analyses have been performed on a refined realistic 3D model of a multi-span masonry arch bridge representative of many bridges built in Europe to quantify to which extent different response parameters, including global kinematic parameters (e.g., displacements and

Damage metrics for masonry bridges under scour scenarios

rotations on piers, spandrels and arches, twist at deck level, vertical settlements, etc.) and modal parameters (natural frequencies and mode shapes), are affected by scour.

Two scour scenarios have been considered, a local one, involving a single pier, and a global one, involving all piers simultaneously. The response parameters most sensitive to scour have been identified so that they can be used either as damage metrics within a probabilistic framework for performance-based assessments, or for the development of optimal monitoring strategies. Based on the study results, the following kinematic parameters, and relevant monitoring instruments/sensors are recommended:

- Rotations of the upstream face of the piers or spandrel walls, which can be monitored by inclinometers;
- Diagonal relative displacements/strains along the bridge deck. They could be measured using total stations, fiber optics, or other types of transducers;
- Settlements and transversal displacements at the upstream face of the piers and spandrel walls, which can be monitored by total stations, lidars technology, high-resolution cameras, or satellite-based interferometry.

Moreover, this study has confirmed the possibility of detecting scour by monitoring potential changes in the bridge dynamic behaviour. While the changes of vibration frequency become significant only for high levels of scour (such that at least 25% of the base of the foundation is undermined), the changes in transverse mode shapes start to be noticeable since the early stages of the scour process (i.e., before the foundation base starts to be undermined). However, it must be noted that such high sensitivity of the modal shapes is observed only in the case of scour localised at one pier, whereas in the case of scour affecting both piers, significant modal shape variations are observed only when the piers are undermined.

Finally, the model proposed has proven to be suitable to capture the principal damage mechanisms characteristic of the failure of existing masonry arch bridges, from the combined settlement and rotation of the piers to the diagonal cracks development in the arches. According to the outcomes of the presented simulations, damage mechanisms are triggered by levels of excavation underneath the piers of around 30% of the foundation base, while the system failure can be for levels even higher than 50% -60%, depending on the type of scour scenario (global or localised, respectively). Such high level of scour required to lead masonry arch bridges to collapse can be explained by the significant robustness characterising this bridge typology. In fact, it is not uncommon to find cases of bridge still standing with a pier base excavated up to the 80% of its length.

Considering the substantial similarity in shape and size of the bridges falling into the class of structures analysed in this paper, it is expected that the response and the behaviour observed in the present case study under scour actions can be also representative of other similar contexts, at least from a qualitative point of view, while it may be possible, for instance, to observe other bridges failing for lower values of B_s/B . Hence, it may be advisable to extend the study considering bridges with other geometrical and mechanical properties, which reveals a necessary step for the aim, for instance, of developing scour fragility functions for this bridge typology. The provided recommendation about the parameters to be monitored and the optimal sensors location, instead, are expected to be general. Further studies will be aimed to investigate some aspects neglected in this paper, such as scour scenarios corresponding to different angles of attack of the flow, development of vulnerability curves accounting for the various sources of uncertainty relevant to the problem, monitoring-based decision support system for bridge scour risk management, multiple hazards risk analysis (e.g., under combined scour and traffic actions).”

REFERENCES

- [1] Hoffmans GJCM, Verheij HJ. Scour Manual. Routledge; 2017. doi:10.1201/9780203740132.
- [2] Melville BW, Coleman SE. Bridge scour. Water Resources Publications, LLC; 2000.
- [3] Pizarro, A., Manfreda, S., & Tubaldi, E. (2020). The science behind scour at bridge foundations: A review. *Water*, 12(2), 374.
- [4] Smith, D.W. Bridge failures. *Proc. Inst. Civil Eng.* 1976, 60, 367–382.
- [5] Kattell, J.; Eriksson, M. Bridge Scour Evaluation: Screening, Analysis, & Countermeasures; U.S. Department of Agriculture: Washington, DC, USA, 1998.
- [6] Wardhana, K.; Hadipriono, F.C. Analysis of recent bridge failures in the United States. *J. Perform. Constr. Facil.* 2003, 17, 144–150.
- [7] Imam, B.M.; Marios, K. Causes and consequences of metallic bridge failures. *Struct. Eng. Int.* 2012, 22, 93–98.
- [8] Lamb, R., Aspinall, W., Odbert, H., & Wagener, T. (2017). Vulnerability of bridges to scour: insights from an international expert elicitation workshop. *Natural Hazards and Earth System Sciences*, 17(8), 1393-1409.
- [9] Di Dieco, G. D., Barbosa, A. R., & Pregnolato, M. (2022, January). A taxonomy of riverine roadway bridges at risk of flooding: towards bridge classes and damage models. In *Proceedings of the Institution of Civil Engineers-Bridge Engineering* (pp. 1-15). Thomas Telford Ltd.
- [10] Argyroudis, S. A., & Mitoulis, S. A. (2021). Vulnerability of bridges to individual and multiple hazards-floods and earthquakes. *Reliability Engineering & System Safety*, 107564.
- [11] Tubaldi, E., White, C. J., Patelli, E., Mitoulis, S. A., De Almeida, G., Brown, J., ... & Zonta, D. (2022). Invited perspectives: challenges and future directions in improving bridge flood resilience. *Natural Hazards and Earth System Sciences*, 22(3), 795-812.
- [12] Page J. Masonry arch bridges. TRL-State of the art review, Department of Transport 1993.
- [13] Wilmers, W. 2012. "Restoration of masonry arch bridges." In Vol. 165 of *Proc., Institution of Civil Engineers-Bridge Engineering*, 135–146. London: Institution of Civil Engineers.

- [14] O’Keefe, P., and T. Simington. 2016. Stone bridges: History and heritage of masonry arch bridges in Ireland. Newbridge, Ireland: Irish Academic Press.
- [15] NRC (National Research Council). (2008). Potential impacts of climate change on U.S. Transportation (Special Report 290). Washington D.C.: Committee on Climate Change and U.S. Transportation, Transportation Research Board, National Research Council
- [16] Zampieri P, Zanini MA, Faleschini F, Hofer L, Pellegrino C. Failure analysis of masonry arch bridges subject to local pier scour. *Engineering Failure Analysis* 2017;79:371–84. doi:10.1016/J.ENGFAILANAL.2017.05.028.
- [17] Tubaldi E, Macorini L, Izzuddin BA. Three-dimensional mesoscale modelling of multi-span masonry arch bridges subjected to scour. *Engineering Structures* 2018;165:486–500. doi:10.1016/J.ENGSTRUCT.2018.03.031.
- [18] Scozzese, F., Ragni, L., Tubaldi, E., & Gara, F. (2019). Modal properties variation and collapse assessment of masonry arch bridges under scour action. *Engineering Structures*, 199, 109665.
- [19] George, J., & Menon, A. (2021). A mechanism-based assessment framework for masonry arch bridges under scour-induced support rotation. *Advances in Structural Engineering*, 24(12), 2637-2651.
- [20] Mendoza Cabanzo, C., Santamaría, M., Sousa, H. S., & Matos, J. C. (2022). In-Plane Fragility and Parametric Analyses of Masonry Arch Bridges Exposed to Flood Hazard Using Surrogate Modeling Techniques. *Applied Sciences*, 12(4), 1886.
- [21] Link, O., García, M., Pizarro, A., Alcayaga, H., & Palma, S. (2020). Local scour and sediment deposition at bridge piers during floods. *Journal of Hydraulic Engineering*, 146(3), 04020003.
- [22] Tubaldi, E., Macorini, L., Izzuddin, B. A., Manes, C., & Laio, F. (2017). A framework for probabilistic assessment of clear-water scour around bridge piers. *Structural safety*, 69, 11-22.

- [23] Prendergast, L. J., & Gavin, K. (2014). A review of bridge scour monitoring techniques. *Journal of Rock Mechanics and Geotechnical Engineering*, 6(2), 138-149.
- [24] Maroni, A., Tubaldi, E., Ferguson, N., Tarantino, A., McDonald, H., & Zonta, D. (2020). Electromagnetic sensors for underwater scour monitoring. *Sensors*, 20(15), 4096.
- [25] Vardanega, P. J., Gavriel, G., & Pregolato, M. (2021). Assessing the suitability of bridge-scour-monitoring devices. *Proceedings of the Institution of Civil Engineers-Forensic Engineering*, 174(4), 105-117.
- [26] Civera, M., Calamai, G., & Fragonara, L. Z. (2021, April). System identification via Fast Relaxed Vector Fitting for the Structural Health Monitoring of masonry bridges. In *Structures* (Vol. 30, pp. 277-293). Elsevier.
- [27] Sousa JJ, Bastos L. Multi-temporal SAR interferometry reveals acceleration of bridge sinking before collapse. *Natural Hazards and Earth System Sciences* 2013;13:659–67. doi:10.5194/nhess-13-659-2013.
- [28] Bao, T., Swartz, R. A., Vitton, S., Sun, Y., Zhang, C., & Liu, Z. (2017). Critical insights for advanced bridge scour detection using the natural frequency. *Journal of Sound and Vibration*, 386, 116-133.
- [29] Maroni, A., Tubaldi, E., Val, D. V., McDonald, H., & Zonta, D. (2020). Using Bayesian networks for the assessment of underwater scour for road and railway bridges. *Structural Health Monitoring*, 1475921720956579.
- [30] Faulkner, K., Brownjohn, J. M. W., Wang, Y., & Huseynov, F. (2020). Tracking bridge tilt behaviour using sensor fusion techniques. *Journal of Civil Structural Health Monitoring*, 10(4), 543-555.
- [31] Foti S, Sabia D. Influence of Foundation Scour on the Dynamic Response of an Existing Bridge. *Journal of Bridge Engineering* 2011;16:295–304. doi:10.1061/(ASCE)BE.1943-5592.0000146.

- [32] Antonopoulos, C., Tubaldi, E., Carbonari, S., Gara, F., & Dezi, F. (2022). Dynamic behavior of soil-foundation-structure systems subjected to scour. *Soil dynamics and earthquake engineering*, 152, 106969.
- [33] Tubaldi, E., Antonopoulos, C., Mitoulis, S. A., Argyroudis, S., Gara, F., Ragni, L., ... & Anastasiadis, A. (2022). Field tests and numerical analysis of the effects of scour on a full-scale soil–foundation–structural system. *Journal of Civil Structural Health Monitoring*, 1-21.
- [34] Prendergast LJ, Hester D, Gavin K, O’Sullivan JJ. An investigation of the changes in the natural frequency of a pile affected by scour. *Journal of Sound and Vibration* 2013;332:6685–702. doi:10.1016/J.JSV.2013.08.020.
- [35] Wan Mohtar, W. H. M., Muad, A. M., Porhemmat, M., Ab. Hamid, H., & Whayab, S. S. (2021). Measuring scour level based on spatial and temporal image analyses. *Structural Control and Health Monitoring*, 28(1), e2645.
- [36] Pregolato, M., Giordano, P. F., Prendergast, L. J., Vardanega, P. J., & Limongelli, M. P. (2023). Comparison of risk-based methods for bridge scour management. *Sustainable and Resilient Infrastructure*, 1-18.
- [37] Maroni, A., Tubaldi, E., Val, D., McDonald, H., Lothian, S., Riches, O., & Zonta, D. (2019, August). SHM-based Decision Support System for bridge scour management. In 9th International Conference on Structural Health Monitoring of Intelligent Infrastructure.
- [38] Mackie, K. R., and B. Stojadinović. "Performance-based seismic bridge design for damage and loss limit states." *Earthquake engineering & structural dynamics* 36, no. 13 (2007): 1953-1971.
- [39] Minnucci, Lucia, Fabrizio Scozzese, Sandro Carbonari, Fabrizio Gara, and Andrea Dall’Asta. "Innovative Fragility-Based Method for Failure Mechanisms and Damage Extension Analysis of Bridges." *Infrastructures* 7, no. 9 (2022): 122. <https://doi.org/10.3390/infrastructures7090122>

- [40] Zampieri, P., Tetougueni, C. D., & Pellegrino, C. (2021). Nonlinear seismic analysis of masonry bridges under multiple geometric and material considerations: Application to an existing seven-span arch bridge. In *Structures* (Vol. 34, pp. 78-94). Elsevier.
- [41] Abaqus, V. (2014). 6.14 Documentation. Dassault Systemes Simulia Corporation, 651. 2014.
- [42] Milani G, Lourenço PB. 3D non-linear behavior of masonry arch bridges. *Comput Struct* 2012;110–111:133–50. <https://doi.org/10.1016/J.COMPSTRUC.2012.07.008>.
- [43] Gazetas G. Formulas and Charts for Impedances of Surface and Embedded Foundations. *Journal of Geotechnical Engineering* 1991;117:1363–81. doi:10.1061/(ASCE)0733-9410(1991)117:9(1363).
- [44] Harris JM, Whitehouse RJS. Marine scour: Lessons from Nature’s laboratory. In *Scour 766 and Erosion: Proceedings of the 7th International Conference on Scour and Erosion, 767 Perth, Australia, 2-4 December 2014*, p. 19. CRC Press, 2014.
- [45] Maroni, A., Tubaldi, E., McDonald, H., & Zonta, D. (2023). Monitoring-based adaptive water level thresholds for bridge scour risk management. *Reliability Engineering & System Safety*, 109473.
- [46] Kosič, M., Anžlin, A., & Bau’, V. (2022). Flood Vulnerability Study of a Roadway Bridge Subjected to Hydrodynamic Actions, Local Scour and Wood Debris Accumulation. *Water*, 15(1), 129.
- [47] Demir, A., & Caglar, N. (2019). Numerical determination of crack width for reinforced concrete deep beams. *Computers and Concrete, An International Journal*, 27(2), 193-204.
- [48] P. Borlenghi, A. Saisi & C. Gentile (2023). Effects of changing temperature in the vibration-based model updating of a masonry bridge. *Life-Cycle of Structures and Infrastructure Systems: Proceedings Of The Eighth International Symposium On Life-Cycle Civil Engineering (IALCCE 2023)*, 2-6 JULY, 2023, Milan, Italy (1st ed.). CRC Press. <https://doi.org/10.1201/9781003323020>

- [49] Li, H., Li, S., Ou, J., & Li, H. (2010). Modal identification of bridges under varying environmental conditions: temperature and wind effects. *Structural Control and Health Monitoring*, 17(5), 495-512.
- [50] Nettis, A., Massimi, V., Nutricato, R., Nitti, D. O., Samarelli, S., & Uva, G. (2023). Satellite-based interferometry for monitoring structural deformations of bridge portfolios. *Automation in Construction*, 147, 104707.
- [51] Borlenghi, P., D'Angelo, M., Ballio, F., & Gentile, C. (2022). Continuous monitoring of masonry arch bridges to evaluate the scour action. In *Proceedings of the 1st Conference of the European Association on Quality Control of Bridges and Structures: EUROSTRUCT 2021 1* (pp. 400-408). Springer International Publishing.
- [52] Zona, A. (2020). Vision-based vibration monitoring of structures and infrastructures: An overview of recent applications. *Infrastructures*, 6(1), 4.